European Journal of Medicinal Chemistry 103 (2015) 551–562

Contents lists available at ScienceDirect

European Journal of Medicinal Chemistry

journal homepage: http://www.elsevier.com/locate/ejmech

Research paper

Diethylstilbestrol-scaffold-based pregnane X receptor modulators

Žiga Hodnik [a], Tihomir Tomašič [a], Domen Smodiš [a], Claudio D'Amore [b], Lucija Peterlin Mašič [a], Stefano Fiorucci [b, 1], Danijel Kikelj [a, *, 1]

[a] University of Ljubljana, Faculty of Pharmacy, Aškerčeva 7, 1000 Ljubljana, Slovenia
[b] University of Perugia, Dipartimento di Medicina Clinica e Sperimentale, Nuova Facultàdi Medicina e Chirurgia, S. Andrea delle Fratte, 06132 Perugia, Italy

ARTICLE INFO

Article history:
Received 28 April 2015
Received in revised form
21 July 2015
Accepted 4 September 2015
Available online 8 September 2015

Keywords:
Pregnane X receptor
PXR agonist
PXR antagonist
Diethylstilbestrol
Mimetic
Solomonsterol

ABSTRACT

Due to its function as a regulator of drug-metabolizing enzymes and transporters, pregnane X receptor (PXR) represents an important factor involved in drug metabolism. In this work, we describe the discovery of diethylstilbestrol-based PXR modulators, which were designed from marine sulfated steroids with PXR agonistic activity, solomonsterols A and B, and our recently reported bazedoxifene scaffold-derived PXR antagonists. The methylated diethylstilbestrol derivative **1** displayed potent PXR agonistic activity with an EC_{50} value of 10.5 μM, whereas compounds **3**, **4** and **6** (IC_{50} for **6** = 27.4 μM) and diethylstilbestrol (**2**) itself (IC_{50} = 14.6 μM) exhibited PXR antagonistic effects in HepG2 cells. The PXR modulatory effects of the synthesized diethylstilbestrol derivatives were further confirmed by the induction of PXR-regulated CYP3A4 expression with compound **1,** as well as by the inhibition of the rifaximin-promoted up-regulation of CYP3A4 expression with **2** and its derivative **6**.

1. Introduction

The binding of a ligand to a member of a nuclear receptor family initiates a process that results in the induction of enzymes involved in metabolism, growth, homeostasis, reproduction and inflammation [1]. Pregnane X receptor (PXR), a member of the nuclear receptor subfamily NR1I, is activated by lithocholic acid and protects tissues against the toxic effects of bile acids [2]. As a regulator of drug-metabolizing enzymes and transporters, PXR also functions as a xenobiotic sensor and as a leading transcriptional regulator of drug metabolism [3–5].

PXR is predominantly located in the liver, small intestines and colon, where it regulates the expression of phase I drug-metabolizing enzymes, such as CYP2B6, CYP2C8, CYP2C9, CYP2C19 and CYP3A4, and phase II enzymes, such as glutathione-*S*-transferase, acetyltransferase, sulfotransferase, methyltransferase and uridine 5'-diphosphoglucuronosyl-transferase [3]. Furthermore, it also regulates drug elimination by controlling the expression of phase III efflux ATP-binding cassette (ABC) drug transporters, such as breast cancer resistance protein (BCRP), P-glycoprotein (P-gp) and multiple resistance drug protein (MRP) [4].

As a member of the nuclear receptor family, PXR shares common structure with other nuclear receptors, containing a DNA-binding domain and a ligand-binding domain (LBD) [5,6]. The unique LBD of PXR is defined by a spherical and flexible binding pocket that has a volume ranging from 1150 to more than 1600 $Å^3$ and is capable of binding a diverse array of hydrophobic molecules with the ability to form hydrogen bonds [7]. Agonist binding to LBD is followed by the conformational changes of ligand-dependent activation function 2 (AF-2) and subsequent dissociation of corepressor proteins. The binding of transcriptional coactivators, which finalizes the assembly of proteins that bind to promoter regions of its target genes as a heterodimer with the retinoid X receptor, completes the process and initiates the transcription [8]. In contrast, PXR antagonists suppress the transcription of PXR target genes by disrupting the binding of coactivators to the AF-2 region of LBD [8–10].

Inflammatory bowel disease (IBD), comprising ulcerative colitis and Crohn's disease, is ranked as one of the five most frequent gastrointestinal diseases in the USA [11]. A potent PXR agonist rifaximin displays protective effects against IBD in a colon cell line and in a mouse model in which IBD was initiated with trinitrobenzenesulfonic acid or sodium salt of dextran sulfate [12,13]. In contrast, the protective effect of rifaximin was not evident in PXR-

Abbreviations used: ABC, ATP-binding cassette; AF-2, activation function 2; BCRP, breast cancer resistance protein; DES, diethylstilbestrol; MRP, multiple resistance drug protein.

* Corresponding author.
E-mail address: danijel.kikelj@ffa.uni-lj.si (D. Kikelj).

[1] Contributed equally to this work.

http://dx.doi.org/10.1016/j.ejmech.2015.09.005
0223-5234/

null IBD mice [12]. Solomonsterol A, a sulfated sterol with PXR agonistic activity isolated from the marine sponge *Theonella swinhoei*, in a recent study exhibited a protective effect against clinical signs and symptoms of ulcerative colitis in human PXR-transgenic mice, due to the reduction of level of TNFα, a signature cytokine for this disease [14]. Both studies therefore highlight PXR agonists as promising agents for the treatment of inflammatory bowel disease.

The currently known PXR agonists include structurally diverse molecules, such as semisynthetic antibiotic rifaximin [13,15] and the marine sulfated sterols solomonsterol A and solomonsterol B [14,16,17] isolated from *Theonella swinhoei*. Moreover, various marine sterols from *Theonella* sponges and *Sinularia kavarattiensis* [18–20], including preconicasterol, were also reported as PXR agonists recently. The list of PXR agonists also comprises the oxygenated polyketides from *Plakinastrella mamillaris* [21], such as gracilioether J, the calcium channel blockers nicardipine, nifedipine, felodipine and isradipine [22], the anti-inflammatory drug dexamethasone [23], the cholesterol-lowering agent SR12813 and others [24–26] (Fig. 1).

PXR is overexpressed in breast [27], ovarian [28], endometrial [29], prostate [30], colon [31] and osteosarcoma [32] cancer cells, and recent studies highlight PXR as an important player in the multidrug resistance of cancer cells to chemotherapeutic agents [26,30,31,33]. The administration of the potent PXR agonist SR12813 together with the anticancer agent vinblastine or paclitaxel to the prostate cancer cell line PC-3 resulted in decreased efficiency of both anticancer agents, most likely due to the elevated expression of P-gp [30]. In contrast, the chemosensitivity of colorectal cancer cells to irinotecan was increased in the presence of the PXR antagonist sulforaphane, which highlights the potential of PXR antagonists to overcome multidrug resistance in cancer chemotherapy [31].

Although most of the currently known PXR ligands display agonistic activity, a small number of compounds that bind to PXR act as PXR antagonists (Fig. 2). Ecteinascidin-743, the first reported PXR antagonist, suppresses SR12813-and paclitaxel-induced PXR activation [34]. The biguanide antidiabetic agent metformin suppresses PXR-regulated CYP3A4 expression [35], whereas compound SPB3255 (IC_{50} = 850 nM) presents the most potent PXR antagonist identified to date [36]. The list continues with our recently reported bazedoxifene scaffold-based PXR antagonists (compounds **I** and **II**), which suppress PXR-regulated CYP3A4 expression, as well as PXR expression [37]. The lack of success in the structure-based design of novel PXR antagonists illustrates that, in contrast to PXR agonists, the design and discovery of PXR antagonists presents a demanding task due to the difficult combination of fitting a large and flexible binding pocket and/or binding to a presently unknown part of the receptor surface [8,38]. Indeed, recent studies propose that, in addition to the binding pocket, the AF-2 helix could provide a surface for the binding of the PXR antagonists coumestrol [39] and ketoconazole [9].

In the present work, we report the discovery of novel diethylstilbestrol-derived PXR modulators by application of a combination of ligand-based design, scaffold hopping and steroidomimetic approach to the PXR agonistic-marine sulfated steroids solomonsterols A and B [16] and to our recently reported bazedoxifene-scaffold-based PXR antagonists [37]. The strategy involved the substitution of the steroid core of solomonsterols A and B with synthetically more favorable scaffold of diethylstilbestrol (DES), which is a well-known steroidomimetic surrogate in synthetic estrogens (Figure S1) [40,41] and offers manifold derivatization opportunities at both hydroxyl groups. Furthermore, to study the structure-activity relationship of the DES-based analogs as PXR modulators, we evaluated the impact of (*i*) sulfate ester formation, (*ii*) O-alkylation at both hydroxyl groups, (*iii*) acetylation of the terminal hydroxyl groups and (*iv*) length of the alkylene linker at positions 4 and 4′ of the DES scaffold on modulation of PXR (Fig. 3A).

The study performed in HepG2 cell line revealed diethylstilbestrol dimethyl ether (**1**) as a potent PXR agonist, whereas DES (**2**) itself and the DES derivatives **3**, **4** and **6**, with *O*-acetoxyalkyl and *O*-hydroxyalkyl side chains of varying length displayed PXR antagonistic activity. In contrast to previous studies, which reported DES as a weak PXR agonist with the ability to increase CYP3A4 expression in DPX2 and HG_5LN cells [42–44], surprisingly, DES was identified as a potent PXR antagonist in our assay using the PXR-transfected HepG2 cell line. Beside identification of novel micromolar PXR agonist **1** and novel PXR antagonists **3**, **4** and **6**, this study highlights suitability of diethylstilbestrol scaffold and steroidomimetic approach for design of PXR modulators.

2. Results and discussion

2.1. Design

Solomonsterols A and B, isolated from *Theonella swinhoei*, are marine sulfated steroids possessing PXR agonistic activity [16]. Using a steroidomimetic approach, we have recently replaced their steroid scaffold by the 3-methyl-2-phenyl-1*H*-indole moiety and discovered their non-sulfated analogs displaying PXR antagonistic activity [37]. In the present study, combining the steroidomimetic and scaffold hopping approach, we have replaced the steroid core of solomonsterols A and B by diethylstilbestrol, a well-

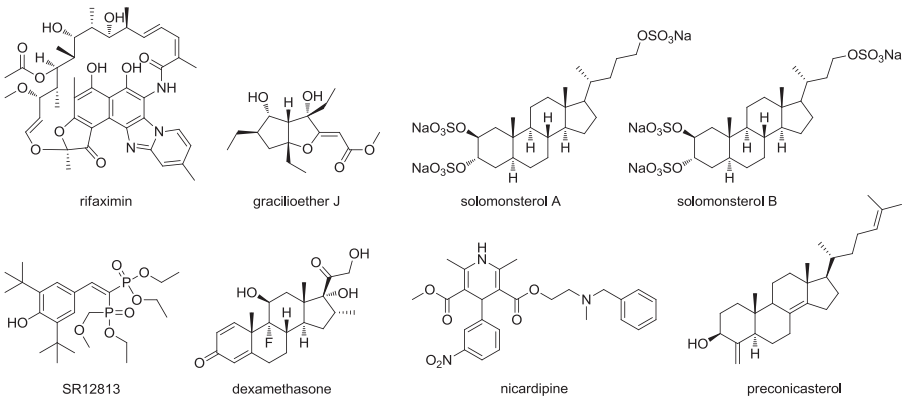

Fig. 1. Structures of some PXR agonists.

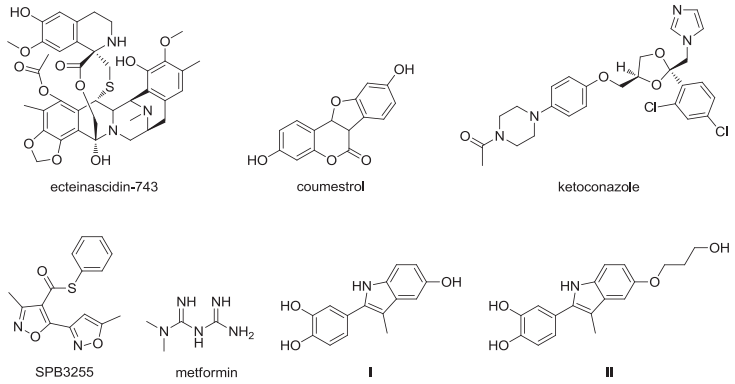

Fig. 2. Structures of currently known PXR antagonists.

known steroidomimetic surrogate (Figure S1), to obtain a focused library of analogs of PXR agonists solomonsterols A and B and of our bazedoxifene-based PXR antagonists (Fig. 3A). Since solomonsterols A and B displayed PXR agonistic activity and their non-sulfated bazedoxifene-scaffold-based analogs possessed PXR antagonistic activity, we have designed and synthesized both their non-sulfated (**2**–**8**) and sulfated (**9**–**12**) DES-scaffold-based analogs (Scheme 1) and evaluated them for PXR agonistic and antagonistic activities. The three-dimensional similarity of the designed DES-scaffold-based PXR modulators, solomonsterol B and bazedoxifene-scaffold-based PXR antagonist **I** was studied using the ROCS (OpenEye Scientific Software, Inc.) [45–47] method of molecular shape and atom type comparison. The ROCS results (Table S1 in the Supporting Information) showed that DES (**2**) overlays well with the bazedoxifene-scaffold-based antagonist **I**, thus highlighting the DES scaffold as appropriate for the design of novel PXR modulators (Fig. 3B). Moreover, the sulfated DES analog **10** (n = 2, R = SO_3–Na^+) displayed good shape similarity to solomonsterol B with a good overlay of alkyl chains bearing a sulfate group with the only difference on the left-hand side of the molecules, where one of the sulfate moieties of solomonsterol B does not have its counterpart in DES derivative **10** (Fig. 3C). Overall, designed compounds **2**–**12** share better shape than color similarity to compound **I** and solomonsterols A and B

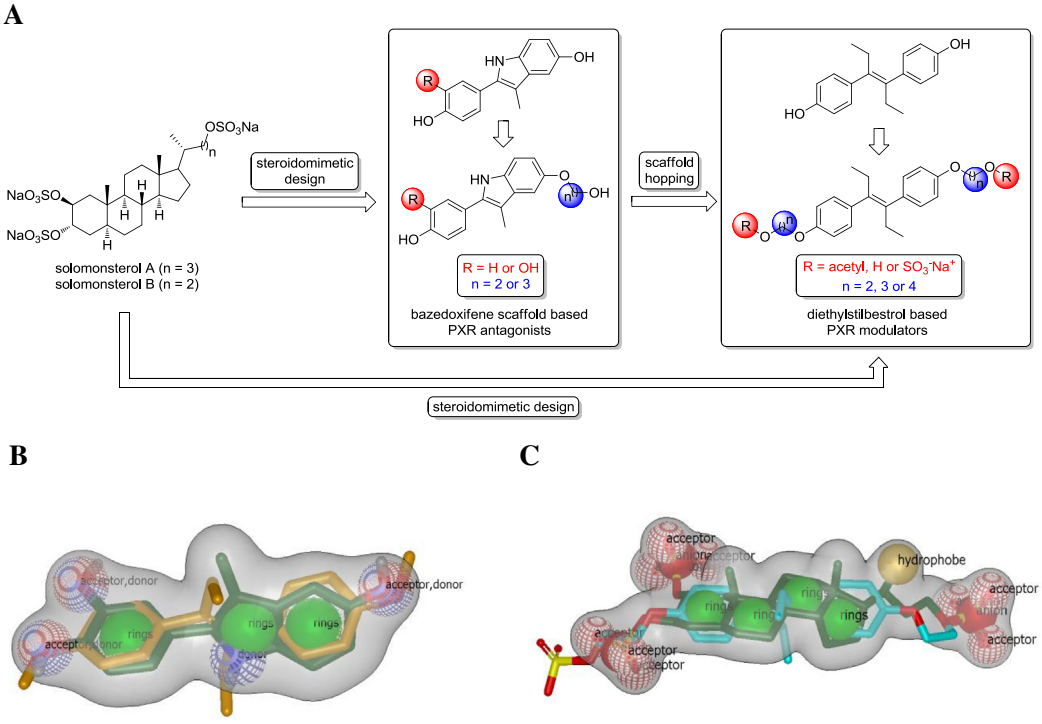

Fig. 3. (A) Design of the diethylstilbestrol-scaffold-based PXR modulators starting from the PXR agonists solomonsterols A and B [16] and our recently discovered bazedoxifene scaffold-based PXR antagonists [37]. (B) Overlay of bazedoxifene-scaffold-based PXR antagonist **I** (for structure see Fig. 2) with diethylstilbestrol (**2**; in *orange*). Compound **I** is represented by *green* sticks, its corresponding shape is shown in *grey*, and its pharmacophoric features are colored *red* for H-bond acceptors, *blue* for H-bond donors and *green* for rings. (**C**) Overlay of solomonsterol B with the designed diethylstilbestrol-scaffold-based PXR modulator **10** (n = 2, R = SO_3–Na^+) in *cyan*. Solomonsterol B is represented by *green* sticks, its corresponding shape is shown in *grey*, and its pharmacophoric features are colored *red* for H-bond acceptors, *blue* for H-bond donors, *green* for rings and *yellow* for hydrophobic groups. Both overlays were obtained using ROCS (OpenEye Scientific Software, Inc.) [45–47]. (For interpretation of the references to colour in this figure legend, the reader is referred to the web version of this article.)

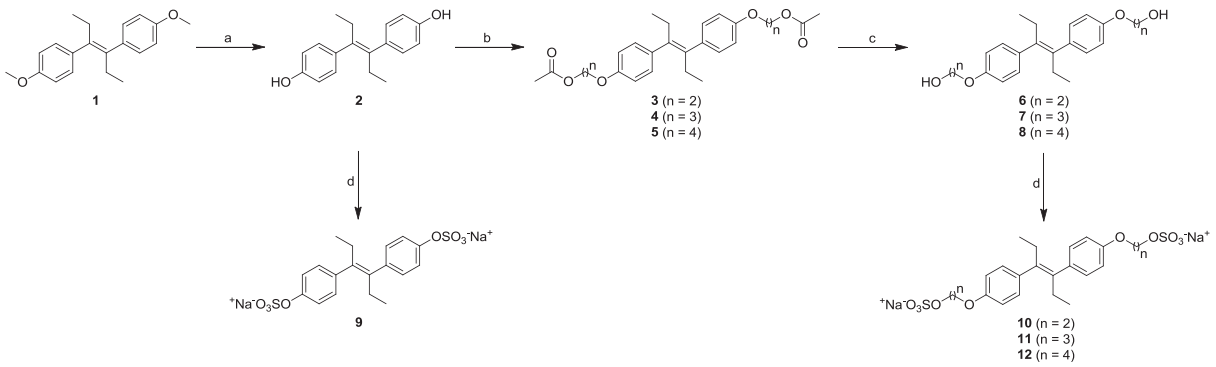

Scheme 1. Reagents and conditions: (*a*) BBr_3, CH_2Cl_2, −78 °C, then rt, 2 h; (*b*) for compound **3**: 2-bromoethyl acetate, Cs_2CO_3, acetone, 60 °C, 48 h; for compound **4**: 3-chloropropyl acetate, NaH, DMF, 60 °C, 18 h; for compound **5**: 4-bromobutyl acetate, Cs_2CO_3, acetone, 60 °C, 48 h; (*c*) 1 M NaOH, MeOH, rt, 2 h; (*d*) chlorosulfonic acid, pyridine, rt, 24 h; then NaOH, pyridine, rt, 24 h.

(Table S1 in the Supporting Information).

2.2. Chemistry

In order to obtain DES (**2**) as the key intermediate in the synthesis of the envisaged series of derivatives to explore the structure-activity relationship, the methyl ether-protected compound **1** was synthesized as previously described [48]. The latter was *O*-deprotected with boron tribromide in dichloromethane to give **2** in good yield. The acetyl-protected DES derivatives **3** and **5** were obtained in a reaction of **2** with the corresponding bromoalkyl acetates and cesium carbonate as the base. The acetyl-protected DES derivative **4** was synthesized in a similar manner using 3-chloropropyl acetate and sodium hydride as the base because cesium carbonate did not yield any product in this case. The subsequent hydrolysis of diesters **3**–**5** yielded *O*-hydroxyalkyl derivatives **6**–**8**. DES (**2**) and compounds **6**–**8** were treated with chlorosulfonic acid in anhydrous pyridine and then subjected to sodium hydroxide-driven salt formation to give sulfate ester salts **9**–**12** in good yields (Scheme 1).

2.3. Biological evaluation

Because solomonsterols A and B have been identified as PXR agonists [16] and our previously reported bazedoxifene scaffold-based analogs displayed PXR antagonistic activity [37], we evaluated DES (**2**) and its derivatives **1** and **3**–**12** for PXR agonistic, as well as for PXR antagonistic activity. A luciferase reporter assay was performed on a human hepatocarcinoma cell line (HepG2) that was transiently transfected with the pSG5-PXR, pSG5-RXR, pGL4.70-Renilla and pGL3(henance) PXRE vectors (*c.f.* Experimental section).

Among the hydroxylated DES derivatives **6**–**8**, only compounds **7** and **8**, with three and four carbon atoms linkers, displayed a slight activation of PXR, whereas the *O*-acetyl derivatives **3**–**5** did not exhibit any PXR agonistic activity at 10 μM compared with the negative control (Fig. 4A). The sulfated analogs **9**–**12** did not display any PXR agonistic activity either, despite possessing sulfate ester groups similarly to PXR agonists solomonsterols A and B [16]. On the contrary, diethylstilbestrol dimethyl ether (**1**) displayed promising PXR agonistic activity at 10 μM, comparable to that of a potent PXR agonist rifaximin [15], which was used as a positive control. Surprisingly, DES (**2**) was devoid of PXR agonistic activity in HepG2 cells, although previous studies reported DES as a weak PXR agonist in other cell lines [42–44].

The series of compounds **1**–**12** was further tested for PXR antagonism at 50 μM concentration using the luciferase reporter assay with the PXR-transfected HepG2 cell line in the presence of rifaximin (10 μM). In contrast to *O*-methyl-protected DES analog **1**, which was identified as a potent PXR agonist in the first assay, *O*-acetyl-protected derivatives **3** and **4** were identified as promising PXR antagonists (Fig. 4B). This finding suggests that, in combination with both linkers that increase the molecule's length, the ester groups of analogs **3** and **4** could provide interactions with the receptor that are favorable for antagonistic activity. It is also possible that partial ester hydrolysis in the test system could contribute to the observed activity of analogs **3** and **4** because the analog **6** exhibited even more evident PXR antagonistic activity. The analog **6** and especially DES (**2**) present the most potent PXR antagonists in this series of compounds, in agreement with our previous results for bazedoxifene scaffold-based PXR antagonists [37], where the antagonistic activity of hydroxylated compounds was inversely correlated to the length of the molecule. Furthermore, the molecule's length seems to play a role also in cytotoxicity and solubility issues at 50 μM. Morphological analysis revealed the cytotoxicity of hydroxylated analogs **7** and **8**, which possess three- and four-carbon atoms linkers, whereas the *O*-acetyl analog **5** with four-carbon atoms linkers displayed poor solubility. Consequently, both issues resulted in unsuccessful evaluation of the PXR antagonistic activities of analogs **5**, **7** and **8**. Finally, the sulfated analogs **9**–**12** were devoid of any noteworthy PXR antagonistic activity, which is again in agreement with the results of our previous study on bazedoxifene-scaffold-based PXR antagonists, in which *O*-sulfatation was detrimental to antagonistic activity [37]. Taking into account the reported PXR agonistic activity of sulfated sterols solomonsterols A and B measured in the same assay, the failure to observe PXR activity with the sulfated analogs **9**–**12** does not seem to be due to issues involving their cell penetration. Molecular docking of sulfated compounds **9**–**12** predicted interaction between their sulfate groups and Lys210 and Ser247 side chains (Figure S3), similarly as observed in the case of solomonsterols A and B. The important difference leading to the absence of PXR agonistic activity of **9**–**12** might be the lack of interaction with His407, which is formed in the case of solomonsterols A and B.

The agonistic activity of diethylstilbestrol dimethyl ether (**1**) was further quantified by a concentration-response transactivation experiment in HepG2 cells. The concentration-response curve revealed the concentration-dependent agonistic activity of **1** ($EC_{50} = 10.5$ μM), which exhibits a slightly higher potency compared with rifaximin ($EC_{50} = 11.2$ μM) (Fig. 5A). The quantification of the antagonistic activities of DES (**2**) and its derivative **6** was also performed in HepG2 cells. Both compounds exhibited concentration-dependent antagonistic effects with IC_{50} values of 14.6 μM and 27.4 μM, respectively (Fig. 5B and C). The higher potency of DES (**2**)

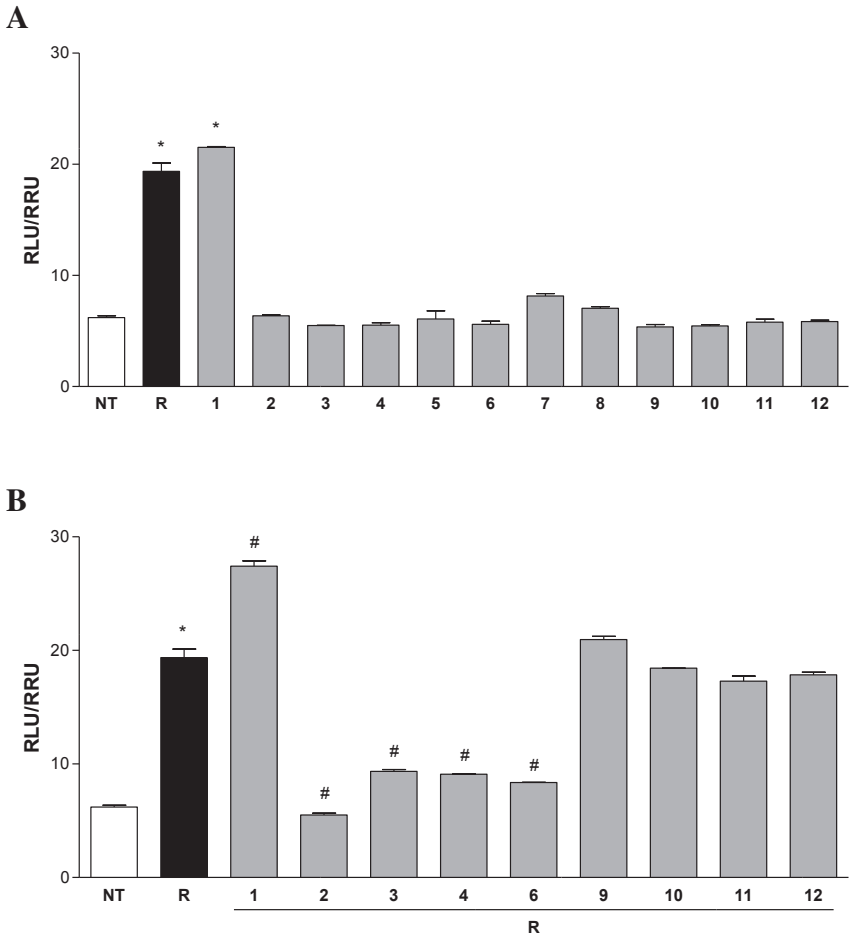

Fig. 4. (A) Luciferase reporter assay performed in HepG2 cells transiently transfected with the full-length PXR, RXR, Renilla and canonical PXRE vectors and stimulated for 18 h with rifaximin (R) alone or **1**–**12** (10 μM) and (B) with 10 μM rifaximin (R) alone or in combination with **1**–**12** (50 μM; results not shown for **5** due to its poor solubility and for **7** and **8** due to detected cytotoxicity).*$p < 0.05$ *vs.* non-treated (NT); #$p < 0.05$ *vs.* rifamimin (R).

compared to its O-substituted derivatives correlates with the results for our recently reported series of bazedoxifene scaffold-based PXR antagonists [37], in which 4-(5-hydroxy-3-methyl-1*H*-indol-2-yl) benzene-1,2-diol (**I**; $IC_{50} = 11$ μM) was the most potent compound and *O*-hydroxyalkyl groups also lowered the PXR antagonistic activity.

A plausible binding mode of the PXR agonist **1** was studied by docking it to the PXR ligand-binding site using the GOLD [49] software. Whereas the docking of solomonsterol A to the PXR ligand-binding pocket displayed ionic interactions with Lys210 (24-*O*-sulfate), hydrogen bonds with Ser247 (3-*O*-sulfate) and His407 (2-*O*-sulfate), as well as several hydrophobic interactions between the steroidal nucleus and the protein [16,50], the binding of PXR agonist **1** in the PXR ligand-binding pocket showed mostly hydrophobic interactions with the PXR residues and a hydrogen bond between the ligand's methoxy group and Lys210 side chain (Fig. 6). Analysis of all 25 docking poses revealed the presence of two main clusters (RMSD < 1.5 Å) of docking solutions. The first cluster contained 12 docking poses (Figure S2A) similar to the highest ranked pose presented in Fig. 6, where in each case hydrogen bond between Lys210 and one of the methoxy groups was observed. Distance between the remaining methoxy group and Ser247 side chain hydroxyl group was in the range between 3.4 and 4.8 Å, which indicates that hydrogen bond with Ser247 might be present taking into account also the flexibility of the PXR ligand-binding pocket. In the second cluster of 10 docking poses (Figure S2B), which were mostly ranked lower than those of the first cluster, no hydrogen bonds were observed between Lys210, Ser247, His407 and the ligand methoxy groups. Molecular docking calculations of compounds **2**–**12** predicted similar binding of their DES scaffold and the formation of hydrogen bonds with Lys210 and Ser247 and methoxy groups of compounds **3**, **4**, **6**–**12**. Therefore, we were not able to differentiate between active and inactive compounds using our docking protocol.

To further evaluate the determined PXR-antagonistic activity of DES (**2**) and its most potent derivative **6** as well as PXR-agonistic activity of **1**, we measured their effects on the expression of PXR and its primary target gene CYP3A4 (Fig. 7). The real-time PCR analysis, which was performed on cDNA isolated from HepG2 cells, revealed a slightly increased up-regulation of PXR expression by agonist **1** at 10 μM, as compared to that of rifaximin (10 μM). Additionally, compound **1** significantly up-regulated CYP3A4 gene expression, which despite being weaker than that obtained with rifaximin, further illustrates its PXR agonistic potential (Fig. 7A). In contrast to our previously reported bazedoxifene-scaffold-based analogs [37], DES (**2**) and its analog **6** in particular, as PXR antagonists, slightly increased the rifaximin (10 μM)-induced up-regulation of PXR expression at 25 μM. Compounds **2** and **6** also inhibited rifaximin-induced CYP3A4 expression, which highlights their potential to suppress PXR-regulated phase I drug metabolism *in vitro* (Fig. 7B). Furthermore, the inhibition of PXR-regulated CYP3A4 expression confirms the PXR antagonistic effect of DES

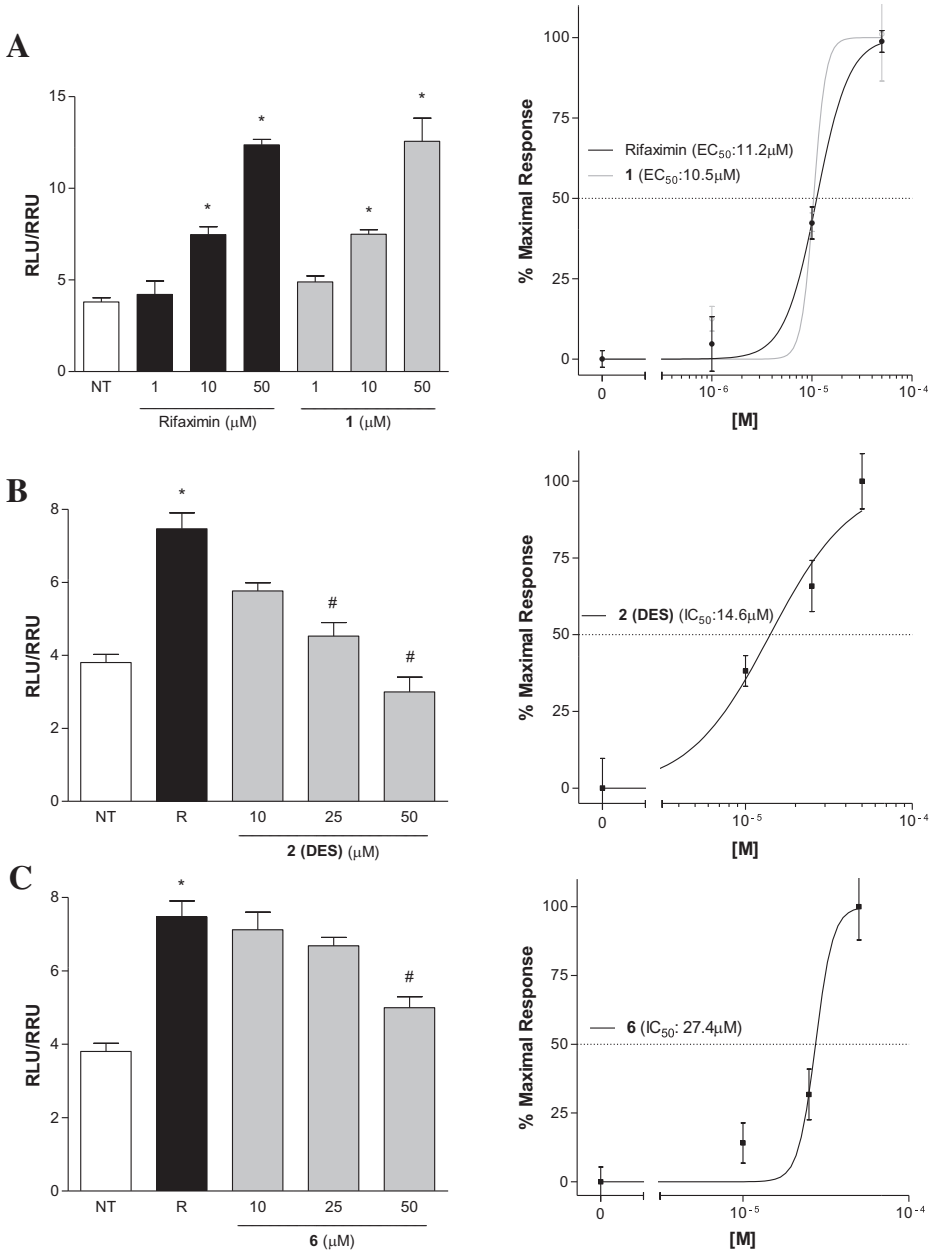

Fig. 5. Concentration-response curves for compounds **1** (A), **2** (B) and **6** (C). HepG2 cells were transfected as described above and stimulated with (A) increasing concentrations of rifaximin or **1** (10 μM) to determine the EC_{50} values or (B, C) with rifaximin (R) alone or in combination with increasing concentrations of **2** or **6** (10, 25 and 50 μM) to determine the IC_{50} values. $^{*}p < 0.05$ *vs.* NT; $\#p < 0.05$ *vs.* rifaximin (R).

(**2**) in HepG2 cells, which is in contrast to the results of previous studies that described DES as a weak PXR agonist in different cell lines [42–44].

Since DES (**2**) is a-well known estrogen receptor agonist and also inhibits estrogen-related receptor β (ERRβ) transcriptional activities [52–54], we have evaluated estrogen receptor α (ERα) and ERRβ binding of compounds **1** and **6** and compared them with the binding data obtained for DES (**2**). A luciferase reporter assay was performed on HepG2 cells transiently transfected with the reporter vectors $p(UAS)_{5X}$-TKLuc, pGL4.70-Renilla and with different vectors containing the ligand binding domain of ERα or ERRβ cloned upstream of the GAL4-DNA binding domain (pSG5-GAL4/ERα and pFN26-GAL4/ERRβ) (*c.f.* Experimental section). The derivative **6** displayed ERα agonism but activation of ERα at 10 μM was weaker as compared to DES (**2**) or 17β-estradiol. On the other hand, diethylstilbestrol dimethyl ether (**1**) did not display any ERα agonistic activity at 10 μM (Fig. 8A), which is in agreement with SAR of natural and synthetic estrogens, claiming the importance of the two hydroxy groups for ERα agonistic activity. Transactivation experiment performed with the ERRβ-transfected HepG2 cells using genistein, a selective ERRβ agonist as a positive control, confirmed that compounds **1**, **2** and **6** do not possess any noteworthy ERRβ agonistic activity at 10 μM (Fig. 8B). The data obtained from the antagonism experiments revealed that at 50 μM compounds **1**, **2** and **6** increased the 17β-estradiol ability to induce ERα activity (Fig. 8C), and reverted the genistein-induced transactivation of ERRβ although compounds **1** and **6** were found less potent antagonists of ERRβ as compared to DES (**2**) (Fig. 8D).

In summary, among identified PXR modulators **1** and **6** derived from diethylstilbestrol (**2**), PXR agonist **1** is devoid of ERα agonistic

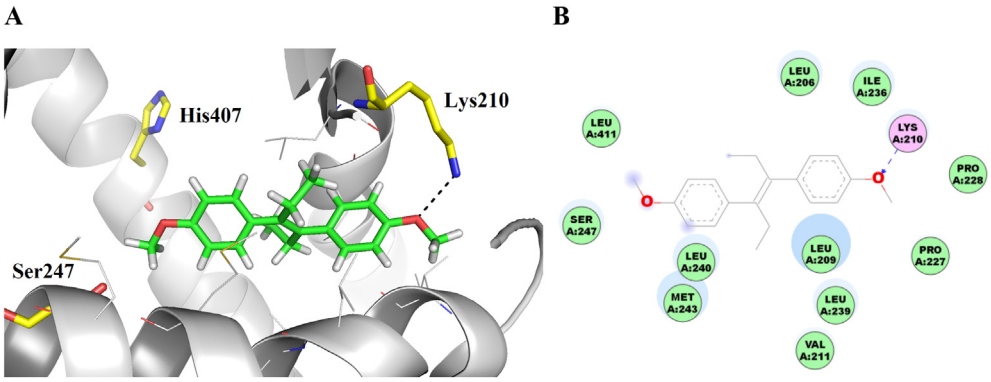

Fig. 6. (A) Highest ranked GOLD-calculated binding pose of PXR agonist **1** (*green* sticks) in the PXR ligand-binding site (*grey*, PDB entry: 1M13). The hydrogen bonds between the ligand and PXR residues (*yellow*) are presented as dashed black lines. The PXR residues forming hydrophobic interactions are presented as *grey* lines. The figure was prepared by PyMOL [51]. (B) 2D diagram of interactions between compound **1** and PXR. The hydrogen bond with Lys210 (*magenta*) is represented in *blue*, and the hydrophobic interactions with PXR residues (*green*) are colored *cyan*. (For interpretation of the references to colour in this figure legend, the reader is referred to the web version of this article.)

activity characteristic for diethylstilbestrol but still retains a weak ERRβ antagonistic activity as compared to DES. The new PXR antagonist **6** possesses weaker ERα agonistic and ERRβ antagonistic activities in comparison to diethylstilbestrol.

3. Conclusion

Replacement of the bazedoxifene core of our previously reported PXR antagonists [37] with the diethylstilbestrol scaffold, as well as the incorporation of the structural motifs of solomonsterols A and B resulted in novel PXR modulators with the ability to alter PXR-regulated CYP3A4 expression. While the methylated analog **1** displayed PXR agonistic activity (EC_{50} = 10.5 μM) comparable to that of rifaximin, analogs **3**, **4** and **6** (IC_{50} for **6** = 27.4 μM) exhibited PXR antagonistic effects in HepG2 cells. Diethylstilbestrol (**2**) itself also displayed dose-dependent PXR antagonistic activity (IC_{50} = 14.6 μM) in HepG2 cells, which was further confirmed by DES-induced inhibition of PXR-regulated CYP3A4 expression. Interestingly, in contrast to these results DES had been identified as a weak PXR agonist in DPX2 and HG_5LN cells [42–44] and therefore it would be interesting to test the library of our DES-scaffold-based analogs also in these cell lines. As some H-bond donor and acceptor groups were lost in the DES-scaffold-based compounds, introduction of additional hydroxyl groups on the phenyl rings of the DES scaffold could be beneficial to increase activity of these compounds on PXR. In comparison with diethylstilbestrol, the PXR agonist **1** and PXR antagonist **6** possess weaker estrogen receptor α agonistic and estrogen-related receptor β antagonistic activities, making them and diethylstilbestrol scaffold good starting points for further elaboration toward selective PXR modulators.

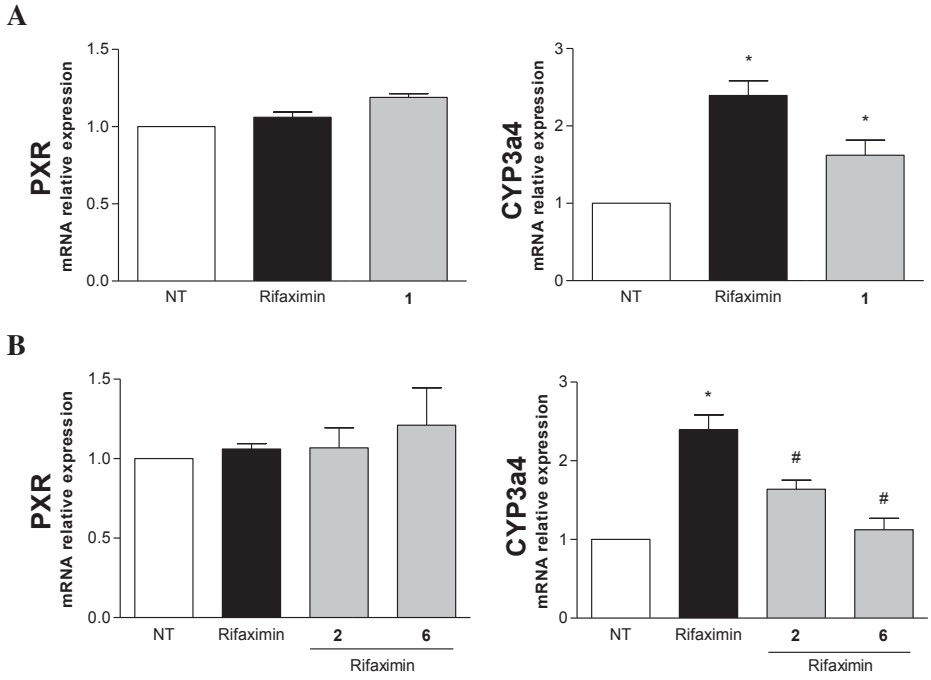

Fig. 7. Real-time PCR analysis of the mRNA relative expression of PXR and its target gene CYP3A4. HepG2 cells were treated (A) with rifaximin (10 μM) or **1** (10 μM) and (B) with rifaximin (10 μM) alone or in combination with DES (**2**) or **6** (25 μM). The values are normalized relative to the level of GAPDH mRNA and are expressed relative to those levels obtained in non-treated cells (NT), which were arbitrarily set to 1. *$p < 0.05$ *vs.* NT; #$p < 0.05$ *vs.* rifaximin.

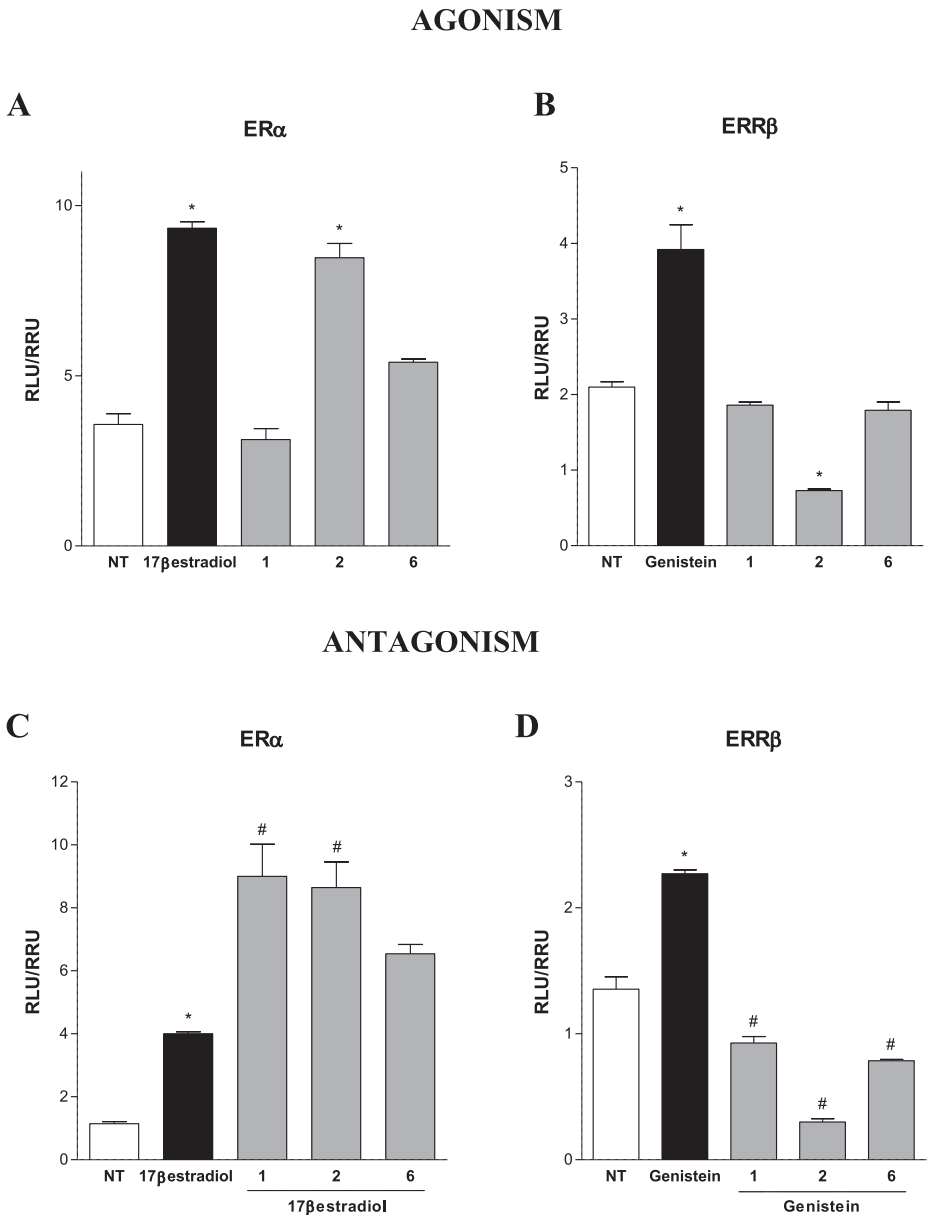

Fig. 8. Luciferase reporter assay performed in HepG2 cells transiently transfected with (A, C) pSG5-GAL4/ERα and p(UAS)$_{5x}$-TKLuc or (B, D) pFN26-GAL4/ERRβ and p(UAS)$_{5x}$-TKLuc, stimulated for 18 h (A) with 17β-estradiol,**1**, **2** or **6** (10 μM), (B) with genistein, **1**, **2** or **6** (10 μM), (C) with 10 μM 17β-estradiol alone or in combination with **1**, **2** or **6** (50 μM), and (D) with 10 μM genistein alone or in combination with **1**, **2** or **6** (50 μM). *p < 0.05 vs. non-treated (NT); #p < 0.05 vs. 17β-estradiol or genistein.

4. Experimental section

4.1. General procedures

All reagents were used as received from commercial sources without further purification unless otherwise indicated. Analytical TLC was performed on Merck silica gel (60 F 254) plates (0.25 mm) and components visualized with staining reagents or UV light. Column chromatography was carried out on silica gel 60 (particle size 240–400 mesh). Reversed-phase column chromatography was performed on Biotage Isolera One system, using Biotage SNAP KP-C18-HS cartridge. HPLC analyses were performed on Agilent Technologies 1100 instrument with G1365B UV–VIS detector, G1316A thermostat and G1313A autosampler using Agilent Eclipse Plus C18 column (5 μm, 4.6 × 150 mm). Three different methods were used for HPLC analyses: *Method A*: Agilent 5μ C18 column; mobile phase: 0.1% trifluoroacetic acid in water (A) and methanol (B); gradient: 90% A to 30% A in 20 min, then 10 min 30% A; flow rate 1.0 mL/min; injection volume: 10 μL; *Method B*: Agilent 5μ C18 column; mobile phase: water (A) and methanol (B); gradient: 70% A to 10% A in 15 min, then 5 min 10% A; flow rate 1.0 mL/min; injection volume: 10 μL; *Method C*: Agilent 5μ C18 column; mobile phase: 20 mM phosphate buffer (pH 7.0) (A) and methanol (B); gradient: 70% A to 30% A in 15 min, then 5 min 30% A; flow rate 1.0 mL/min; injection volume: 10 μL. All tested compounds were ≥95% pure by HPLC. ^{1}H NMR and ^{13}C NMR spectra were recorded at 400 MHz and 101 MHz, respectively, on a Bruker AVANCE III spectrometer in DMSO-d_6, CD_3OD or $CDCl_3$ solution with TMS as an internal standard at 25 °C. Spectra were assigned using gradient COSY, HSQC and DEPT experiments. IR spectra were recorded on a Thermo Nicolet Nexus 470 ESP FT-IR spectrometer. Mass spectra were obtained using a VG Analytical Autospec Q mass

spectrometer. Microanalyses were performed on a Perkin–Elmer C,H,N analyzer 2400 II. All reported yields are yields of purified products.

4.2. Synthesis

4.2.1. (E)-4,4′-(Hex-3-ene-3,4-diyl)bis(methoxybenzene) (**1**).

Synthesized as previously described [48] Colorless oil; IR (ATR) ν 2960, 2931, 2870, 2834, 1606, 1506, 1463, 1286, 1240, 1174, 1034, 823 cm^{-1}; ^1H NMR (400 MHz, DMSO-d_6) δ 0.87 (t, 6H, J = 7.4 Hz, 2 × CH_3), 2.48 (q, 4H, J = 7.4 Hz, 2 × CH_2, signal overlapped with DMSO-d_5), 3.65 (s, 6H, 2 × CH_3), 6.64–6.68 (m, 4H, 4 × Ar–H), 6.84–6.88 (m, 4H, 4 × Ar–H) ppm; ^{13}C NMR (101 MHz, DMSO-d_6) δ13.19 (2C), 26.91 (2C), 54.72 (2C), 112.93 (4C), 130.45 (4C), 134.89 (2C), 137.52 (2C), 156.87 (2C) ppm. HRMS m/z for $C_{20}H_{24}O_2$ ($[M + H^+]^+$): calcd 297.1855; found 297.1858. Elemental analysis calculated (%) for $C_{20}H_{24}O_2$: C 81.04, H 8.16. Found: C: 80.85, H 8.11.

4.2.2. (E)-4,4′-(Hex-3-ene-3,4-diyl)diphenol (**2**)

The solution of (*E*)-4,4′-(hex-3-ene-3,4-diyl)bis(methoxybenzene) (**1**) (6.42 g, 22.0 mmol) in dry CH_2Cl_2 (150 mL) was cooled to −78 °C and then BBr_3 (6.36 mL, 66.0 mmol) was added dropwise under argon atmosphere. The mixture was then stirred for 2 h at room temperature and poured into the mixture of ice/H_2O (350 mL). The mixture was stirred for 30 min and extracted with CH_2Cl_2 (2 × 200 mL). Combined organic phases were washed with brine (1 × 300 mL), dried over Na_2SO_4 and concentrated under reduced pressure. The crude product was then purified by column chromatography with ethyl acetate/hexane as an eluent to afford compound **2** as an off-white solid. Yield: 3.66 g (63%); IR (ATR) ν 3405, 2975, 2931, 1608, 1589, 1509, 1426, 1335, 1245, 1199, 1171, 829, 805 cm^{-1}; ^1H NMR (400 MHz, DMSO-d_6) δ 0.71 (t, 6H, J = 7.4 Hz, 2 × CH_3), 2.07 (q, 4H, J = 7.4 Hz, 2 × CH_2), 6.74–6.79 (m, 4H, 4 × Ar–H), 6.96–7.01 (m, 4H, 4 × Ar–H), 9.33 (s, 2H, 2 × OH) ppm; ^{13}C NMR (101 MHz, DMSO-d_6) δ 13.32 (2C), 28.03 (2C), 114.85 (4C), 129.30 (4C), 132.48 (2C), 137.93 (2C), 155.68 (2C) ppm. HRMS m/z for $C_{18}H_{20}O_2$ ($[M + H^+]^+$): calcd 269.1542; found 269.1545. HPLC: Method B, retention time: 14.93 min (99.9% at 254 nm).

4.2.3. Synthesis of compounds ***3*** and ***5***

To the solution of (*E*)-4,4′-(hex-3-ene-3,4-diyl)diphenol (**2**) (134 mg, 0.5 mmol) in acetone (20 mL) were added cesium carbonate (489 mg, 1.5 mmol) and 2-bromoethyl acetate (116 μL, 1.05 mmol) or 4-bromobutyl acetate (152 μL, 1.05 mmol). The mixture was stirred at 60 °C for 48 h, concentrated *in vacuo* and dissolved in ethyl acetate (50 mL). Solution was washed with 10% citric acid (2 × 50 mL) and brine (1 × 50 mL). Organic phase was dried over Na_2SO_4 and concentrated under reduced pressure. Crude product was then purified by column chromatography with dichloromethane/methanol (40:1) as an eluent to afford compound **3** or **5**.

4.2.3.1. (E)-((Hex-3-ene-3,4-diylbis(4,1-phenylene))bis(oxy))bis(ethane-2,1-diyl) diacetate (***3***).

Yield: 183 mg (83%); white solid; IR (ATR) ν2958, 2929, 2869, 1736, 1607, 1508, 1466, 1368, 1233, 1176, 1047, 960, 821 cm^{-1}; ^1H NMR (400 MHz, $CDCl_3$) δ 0.78 (t, 6H, J = 7.4 Hz, 2 × CH_3), 2.14 (q, 4H, J = 7.4 Hz, 2 × CH_2), 2.14 (s, 6H, 2 × CH_3), 4.20–4.25 (m, 4H, 2 × CH_2), 4.45–4.49 (m, 4H, 2 × CH_2), 6.92–6.97 (m, 4H, 4 × Ar–H), 7.12–7.17 (m, 4H, 4 × Ar–H) ppm; ^{13}C NMR (101 MHz, $CDCl_3$) δ 13.39 (2C), 20.97 (2C), 28.58 (2C), 62.98 (2C), 65.86 (2C), 114.08 (4C), 129.81 (4C), 135.53 (2C), 138.71 (2C), 156.88 (2C), 171.10 (2C) ppm. HRMS m/z for $C_{26}H_{32}O_6$ ($[M + H^+]^+$): calcd 441.2277; found 441.2271. Elemental analysis calculated (%) for $C_{26}H_{32}O_6$: C 70.89, H 7.32. Found: C: 70.79, H 7.43.

4.2.3.2. (E)-((Hex-3-ene-3,4-diylbis(4,1-phenylene))bis(oxy))bis(butane-4,1-diyl) diacetate (***5***).

Yield: 213 mg (86%); white solid; IR (ATR) ν 2982, 2953, 2929, 2869, 1732, 1608, 1531, 1472, 1364, 1241, 1178, 1060, 1034, 949, 841, 810 cm^{-1}; ^1H NMR (400 MHz, $CDCl_3$) δ 0.79 (t, 6H, J = 7.4 Hz, 2 × CH_3), 1.83–1.95 (m, 8H, 4 × CH_2), 2.08 (s, 6H, 2 × CH_3), 2.15 (q, 4H, J = 7.4 Hz, 2 × CH_2), 4.04 (t, 4H, J = 6.0 Hz, 2 × CH_2), 4.18 (t, 4H, J = 6.0 Hz, 2 × CH_2), 6.88–6.93 (m, 4H, 4 × Ar–H), 7.11–7.15 (m, 4H, 4 × Ar–H) ppm; ^{13}C NMR (101 MHz, $CDCl_3$) δ 13.43 (2C), 21.03 (2C), 25.45 (2C), 25.98 (2C), 28.59 (2C), 64.21 (2C), 67.16 (2C), 113.89 (4C), 129.74 (4C), 135.06 (2C), 138.72 (2C), 157.32 (2C), 171.26 (2C) ppm. HRMS m/z for $C_{30}H_{40}O_6$ ($[M + H^+]^+$): calcd 497.2903; 497.2895 found. Elemental analysis calculated (%) for $C_{30}H_{40}O_6$: C 72.55, H 8.12. Found: C: 72.28, H 8.28.

4.2.4. (E)-((Hex-3-ene-3,4-diylbis(4,1-phenylene))bis(oxy))bis(propane-3,1-diyl) diacetate (***4***)

(*E*)-4,4′-(Hex-3-ene-3,4-diyl)diphenol (**2**) (188 mg, 0.7 mmol) was dissolved in DMF (15 mL) and cooled to 0 °C. 95% sodium hydride (32 mg, 1.4 mmol) was added and the solution was stirred for 30 min at room temperature. Reaction mixture was cooled to 0 °C again and 3-chloropropyl acetate (180 μL, 1.47 mmol) was added. The mixture was stirred for 18 h at 60 °C, concentrated *in vacuo* and suspended in ethyl acetate (50 mL). Suspension was washed with water (1 × 40 mL), 10% citric acid (1 × 40 mL) and brine (1 × 40 mL). Organic phase was dried over Na_2SO_4 and the solvent was removed under reduced pressure. The crude product was then purified by column chromatography with dichloromethane/methanol (40:1) as an eluent to afford **4** as white solid. Yield: 200 mg (61%); IR (ATR) ν 2950, 2929, 2869, 1739, 1607, 1510, 1467, 1367, 1230, 1175, 1046, 960, 821 cm^{-1}; ^1H NMR (400 MHz, $CDCl_3$) δ 0.79 (t, 6H, J = 7.4 Hz, 2 × CH_3), 2.10 (s, 6H, 2 × CH_3), 2.11–2.18 (m, 8H, 4 × CH_2), 4.10 (t, 4H, J = 6.2 Hz, 2 × CH_2), 4.31 (t, 4H, J = 6.2 Hz, 2 × CH_2), 6.89–6.94 (m, 4H, 4 × Ar–H), 7.11–7.16 (m, 4H, 4 × Ar–H) ppm; ^{13}C NMR (101 MHz, $CDCl_3$) δ 13.43 (2C), 21.02 (2C), 28.60 (2C), 28.71 (2C), 61.41 (2C), 64.19 (2C), 113.92 (4C), 129.75 (4C), 135.18 (2C), 138.72 (2C), 157.18 (2C), 171.14 (2C) ppm. HRMS m/z for $C_{28}H_{36}O_6$ ($[M + H^+]^+$): calcd 469.2590; found 469.2579. Elemental analysis calculated (%) for $C_{28}H_{36}O_6$: C 71.77, H 7.74. Found: C: 71.56, H 7.81.

4.2.5. Synthesis of compounds ***6***–***8***

Compound **3**, **4** or **5** (0.35 mmol) was dissolved in methanol (20 mL) and cooled to 0 °C. 1 M $NaOH_{(aq)}$ (3.5 mL, 3.5 mmol) was added dropwise and the mixture was stirred for 2 h at room temperature. Reaction mixture was concentrated *in vacuo*, dissolved in ethyl acetate (50 mL) and washed with 10% citric acid 2 × 40 mL) and brine (1 × 50 mL). Organic phase was dried over Na_2SO_4 and concentrated under reduced pressure to yield compound **6**, **7** or **8**.

4.2.5.1. (E)-2,2′-((Hex-3-ene-3,4-diylbis(4,1-phenylene))bis(oxy))diethanol (***6***).

Prepared from (*E*)-((hex-3-ene-3,4-diylbis(4,1-phenylene))bis(oxy))bis(ethane-2,1-diyl) diacetate (**3**) (154 mg, 0.35 mmol) according to general procedure. Yield: 110 mg (88%); white solid; IR (ATR) ν 3471, 2964, 1608, 1509, 1454, 1218, 1072, 1027, 933 cm^{-1}; ^1H NMR (400 MHz, $CDCl_3$) δ 0.79 (t, 6H, J = 7.4 Hz, 2 × CH_3), 2.15 (q, 4H, J = 7.4 Hz, 2 × CH_2), 3.99–4.03 (m, 4H, 2 × CH_2), 4.12–4.16 (m, 4H, 2 × CH_2), 6.92–6.97 (m, 4H, 4 × Ar–H), 7.12–7.17 (m, 4H, 4 × Ar–H) ppm; ^{13}C NMR (101 MHz, $CDCl_3$) δ 13.41 (2C), 28.59 (2C), 61.59 (2C), 69.11 (2C), 114.05 (4C), 129.82 (4C), 135.49 (2C), 138.72 (2C), 157.03 (2C) ppm. HRMS m/z for $C_{22}H_{28}O_4$ ($[M + H^+]^+$): calcd 357.2066; found 357.2056. HPLC: Method A, retention time: 26.44 min (98.3% at 254 nm).

4.2.5.2. (E)-3,3′-((Hex-3-ene-3,4-diylbis(4,1-phenylene))bis(oxy))bis(propan-1-ol) (***7***).

Prepared from (*E*)-((hex-3-ene-3,4-diylbis(4,1-phenylene))bis(oxy))bis(propane-3,1-diyl) diacetate (**4**)

(164 mg, 0.35 mmol) according to general procedure. Yield: 121 mg (90%); white solid; IR (ATR) ν 3600, 3498, 2953, 2869, 1732, 1608, 1512, 1472, 1364, 1237, 1178, 1032, 950, 841 cm^{-1}; ^1H NMR (400 MHz, DMSO-d_6) δ 0.72 (t, 6H, $J = 7.4$ Hz, 2 × CH_3), 1.88 (p, 4H, $J = 6.3$ Hz, 2 × CH_2), 2.09 (q, 4H, $J = 7.4$ Hz, 2 × CH_2), 3.55–3.61 (m, 4H, 2 × CH_2), 4.05 (t, 4H, $J = 6.3$ Hz, 2 × CH_2), 4.57 (t, 2H, $J = 5.2$ Hz, 2 × OH), 6.92–6.97 (m, 4H, 4 × Ar–H), 7.09–7.14 (m, 4H, 4 × Ar–H) ppm; ^{13}C NMR (101 MHz, DMSO-d_6) δ 13.25 (2C), 28.01 (2C), 32.17 (2C), 57.29 (2C), 64.32 (2C), 113.97 (4C), 129.38 (4C), 133.88 (2C), 137.95 (2C), 157.15 (2C) ppm. HRMS *m/z* for $C_{24}H_{32}O_4$ ($[M + H^+]^+$): calcd 385.2379; found 385.2369. HPLC: Method B, retention time: 17.55 min (98.1% at 254 nm).

*4.2.5.3. (E)-4,4′-((Hex-3-ene-3,4-diylbis(4,1-phenylene))bis(oxy)) bis(butan-1-ol) (**8**).* Prepared from (*E*)-((hex-3-ene-3,4-diylbis(4,1-phenylene))bis(oxy))bis(butane-4,1-diyl) diacetate (**5**) (174 mg, 0.35 mmol) according to general procedure. Yield: 125 mg (87%); off-white solid; IR (ATR) ν 3291, 2948, 2868, 1607, 1509, 1460, 1243, 1173, 1049, 970, 831 cm^{-1}; ^1H NMR (400 MHz, $CDCl_3$) δ 0.79 (t, 6H, $J = 7.4$ Hz, 2 × CH_3), 1.77–1.85 (m, 4H, 2 × CH_2), 1.90–1.98 (m, 4H, 2 × CH_2), 2.15 (q, 4H, $J = 7.4$ Hz, 2 × CH_2), 3.78 (t, 4H, $J = 6.2$ Hz, 2 × CH_2), 4.06 (t, 4H, $J = 6.2$ Hz, 2 × CH_2), 6.90–6.94 (m, 4H, 4 × Ar–H), 7.11–7.16 (m, 4H, 4 × Ar–H) ppm; ^{13}C NMR (101 MHz, $CDCl_3$) δ 13.43 (2C), 25.95 (2C), 28.59 (2C), 29.63 (2C), 62.63 (2C), 67.69 (2C), 113.93 (4C), 129.75 (4C), 135.11 (2C), 138.71 (2C), 157.25 (2C) ppm. HRMS *m/z* for $C_{26}H_{36}O_4$ ($[M + H^+]^+$): calcd 413.2692; found 413.2684. HPLC: Method B, retention time: 18.40 min (99.9% at 254 nm).

*4.2.6. Synthesis of compounds **9**–**12***

Compound **2**, **6**, **7** or **8** (0.25 mmol) was dissolved in anhydrous pyridine (10 mL) under argon atmosphere and the solution was cooled to −16 °C. Chlorosulfonic acid (330 μL, 5.0 mmol) was added dropwise and the yellow suspension was stirred at room temperature for 24 h. The suspension was cooled to 0 °C and the pH was adjusted to 10 with 5 M $NaOH_{(aq)}$. Reaction mixture was then stirred for 24 h at room temperature and concentrated under reduced pressure. The solid residue was washed with the mixture of methanol and ethanol (1:1) (4 × 30 mL) and the combined organic phases were concentrated *in vacuo*. The crude product was purified by reversed-phase column chromatography with methanol/water as an eluent to afford compounds **9**–**12**.

*4.2.6.1. Sodium (E)-hex-3-ene-3,4-diylbis(4,1-phenylene) bis(sulfate) (**9**).* Prepared from (*E*)-4,4′-(hex-3-ene-3,4-diyl)diphenol (**2**) (66 mg, 0.25 mmol) according to general procedure. Yield: 81 mg (69%); off-white solid; IR (ATR) ν 3567, 2974, 2959, 2359, 2338, 1499, 1250, 1201, 1044, 1014, 861 cm^{-1}; ^1H NMR (400 MHz, DMSO-d_6) δ 0.74 (t, 6H, $J = 7.4$ Hz, 2 × CH_3), 2.10 (q, 4H, $J = 7.4$ Hz, 2 × CH_2), 7.08–7.14 (m, 4H, 4 × Ar–H), 7.15–7.21 (m, 4H, 4 × Ar–H) ppm; ^{13}C NMR (101 MHz, DMSO-d_6) δ 13.23 (2C), 28.03 (2C), 120.06 (4C), 128.70 (4C), 136.49 (2C), 138.08 (2C), 151.92 (2C) ppm. HRMS *m/z* for $C_{18}H_{18}Na_2O_8S_2$ ($[M\text{-}Na^+]^-$): calcd 449.0341; found 449.0333. HPLC: Method A, retention time: 15.69 min (95.7% at 254 nm).

*4.2.6.2. Sodium (E)-((hex-3-ene-3,4-diylbis(4,1-phenylene))bis(oxy)) bis(ethane-2,1-diyl) bis(sulfate) (**10**).* Prepared from (*E*)-2,2′-((hex-3-ene-3,4-diylbis(4,1-phenylene))bis(oxy))diethanol (**6**) (89 mg, 0.25 mmol) according to general procedure. Yield: 99 mg (71%); yellow solid; IR (ATR) ν3538, 2953, 2929, 2869, 2359, 1606, 1508, 1443, 1236, 1177, 1070, 917, 837 cm^{-1}; ^1H NMR (400 MHz, DMSO-d_6) δ 0.69–0.76 (m, 6H, 2 × CH_3), 2.05–2.13 (m, 4H, 2 × CH_2), 4.01–4.07 (m, 4H, 2 × CH_2), 4.11–4.17 (m, 4H, 2 × CH_2), 6.93–6.99 (m, 4H, 4 × Ar–H), 7.10–7.15 (m, 4H, 4 × Ar–H) ppm; ^{13}C NMR (101 MHz, DMSO-d_6) δ 13.27 (2C), 28.01 (2C), 64.24 (2C), 66.56 (2C), 113.98 (4C), 129.42 (4C), 134.07 (2C), 137.95 (2C), 156.90 (2C) ppm. HRMS *m/z* for $C_{22}H_{26}Na_2O_{10}S_2$ ($[M\text{-}Na^+]^-$): calcd 537.0865; found 537.0881. HPLC: Method C, retention time: 13.22 min (96.3% at 254 nm).

*4.2.6.3. Sodium (E)-((hex-3-ene-3,4-diylbis(4,1-phenylene))bis(oxy)) bis(propane-3,1-diyl) bis(sulfate) (**11**).* Prepared from (*E*)-3,3′-((hex-3-ene-3,4-diylbis(4,1-phenylene))bis(oxy))bis(propan-1-ol) (**7**) (96 mg, 0.25 mmol) according to general procedure. Yield: 91 mg (62%); yellow solid; IR (ATR) ν3485, 2964, 2929, 2871, 2360, 1607, 1509, 1471, 1209, 1036, 948, 833 cm^{-1}; ^1H NMR (400 MHz, DMSO-d_6) δ 0.68–0.76 (m, 6H, 2 × CH_3), 1.91 (p, 4H, $J = 6.4$ Hz, 2 × CH_2), 2.09 (q, 4H, $J = 7.4$ Hz, 2 × CH_2), 3.89 (t, 4H, $J = 6.4$ Hz, 2 × CH_2), 4.03 (t, 4H, $J = 6.4$ Hz, 2 × CH_2), 6.92–6.97 (m, 4H, 4 × Ar–H), 7.09–7.14 (m, 4H, 4 × Ar–H) ppm; ^{13}C NMR (101 MHz, DMSO-d_6) δ 13.27 (2C), 28.02 (2C), 29.01 (2C), 62.48 (2C), 64.33 (2C), 113.99 (4C), 129.40 (4C), 133.99 (2C), 137.96 (2C), 157.04 (2C) ppm. HRMS *m/z* for $C_{24}H_{30}Na_2O_{10}S_2$ ($[M\text{-}Na^+]$): calcd 565.1178; found 565.1173. HPLC: Method A, retention time: 21.24 min (99.9% at 254 nm).

*4.2.6.4. Sodium (E)-((hex-3-ene-3,4-diylbis(4,1-phenylene))bis(oxy)) bis(butane-4,1-diyl) bis(sulfate) (**12**).* Prepared from (*E*)-4,4′-((hex-3-ene-3,4-diylbis(4,1-phenylene))bis(oxy))bis(butan-1-ol) (**8**) (103 mg, 0.25 mmol) according to general procedure. Yield: 105 mg (68%); pale brown solid; IR (ATR) ν 3312, 2957, 2928, 2866, 2360, 1608, 1509, 1464, 1233, 1173, 1058, 989, 827 cm^{-1}; ^1H NMR (400 MHz, DMSO-d_6) δ 0.68–0.76 (m, 6H, 2 × CH_3), 1.63–1.72 (m, 4H, 2 × CH_2), 1.72–1.81 (m, 4H, 2 × CH_2), 2.09 (q, 4H, $J = 7.2$ Hz, 2 × CH_2), 3.77 (t, 4H, $J = 6.4$ Hz, 2 × CH_2), 3.99 (t, 4H, $J = 6.4$ Hz, 2 × CH_2), 6.92–6.97 (m, 4H, 4 × Ar–H), 7.08–7.14 (m, 4H, 4 × Ar–H) ppm; ^{13}C NMR (101 MHz, DMSO-d_6) δ 13.27 (2C), 25.53 (2C), 25.76 (2C), 28.02 (2C), 65.14 (2C), 66.97 (2C), 113.99 (4C), 129.38 (4C), 133.91 (2C), 137.96 (2C), 157.12 (2C) ppm. HRMS *m/z* for $C_{26}H_{34}Na_2O_{10}S_2$ ($[M\text{-}Na^+]^-$): calcd 593.1491; found 593.1498. HPLC: Method C, retention time: 17.25 min (99.9% at 254 nm).

4.3. Transactivation assay

HepG2 cells were seeded in 24-wells plates at density of 5 × 10^4 cells/well in Minimum Essential Medium with Earl's salts containing 10% fetal bovine serum (FBS), 1% L-glutamine and 1% penicillin/streptomycin. The transfection experiments were performed using Fugene HD (Promega, Milan, Italy) according to manufacturer specifications. For PXR mediated transactivation, cells were transfected with 75 ng pSG5-hPXRT1, 75 ng pSG5-RXR, 250 ng of the reporter vector pGL3(henance)PXRE, and with 100 ng of pGL4.70 (Promega), a vector encoding the Renilla gene. At 24 h post-transfection, cells were treated for 18 h with rifaximin (10 μM) and compounds **1**–**12** (10 μM), or with the combination of rifaximin (10 μM) plus compounds **1**–**12** (50 μM). In another experimental setting, cells were primed for 18 h with the increasing doses (10, 25 and 50 μM) of rifaximin or compound **1**, or with rifaximin (10 μM) in combination with increasing doses of **2** or **6** (10, 25 and 50 μM). To evaluate ERα or ERRβ transcriptional activity, HepG2 cells were transiently transfected with 250 ng of the reporter vector $p(UAS)_{5X}$-TKLuc, 100 ng of pGL4.70-Renilla and with different vectors (150 ng each) containing the ligand binding domain of ERα or ERRβ cloned upstream of the GAL4-DNA binding domain (pSG5-GAL4/ERα or pFN26-GAL4/ERRβ); cells were primed for 18 h with 17β-estradiol (10 μM), genistein (10 μM) and compounds **1**, **2** and **6** (10 μM), with the combination of 17β-estradiol (10 μM) plus compounds **1**, **2** and **6** (50 μM) or with the combination of genistein (10 μM) plus compounds **1**, **2** and **6** (50 μM). After treatments, 20 μL of cellular lysate were assayed for luciferase activity using the Luciferase Assay System (Promega). Luminescence was measured using GloMax™

20/20 Luminometer (Promega). Luciferase activities were normalized for transfection efficiencies by dividing the Luciferase relative light units (RLU) by Renilla relative lights units (RRU), expressed from cells co-transfected with pGL4.70-Renilla.

4.4. Quantitative real-time PCR

HepG2 cells were seeded in a 6-well plate at 5×10^5 cells/well in Minimum Essential Medium, with Earl's salts containing 10% fetal bovine serum (FBS), 1% L-glutamine and 1% penicillin/streptomycin. After growing to approximately 70% confluence, cells were serum starved for 24 h and then primed with rifaximin (10 μM) or compound **1**, or with the combination of rifaximin (10 μM) plus compound **2** or **6** (25 μM) for 18 h. Total RNA was isolated with TRIzol Reagent (Invitrogen), incubated with DNase I (Invitrogen) and random reverse-transcribed with Superscript II (Invitrogen) according to manufacturer specifications. For quantitative RT-PCR, 10 ng of template was dissolved in a 20 μL solution containing 200 nM of each primer and 10 μL of KAPA SYBR FAST Universal qPCR Kit (KAPA BIOSYSTEMS). All reactions were performed in triplicate on iCycler instrument (Biorad); the thermal cycling conditions were as follows: 3 min at 95 °C, followed by 40 cycles of 95 °C for 15 s, 58 °C for 20 s and 72 °C for 30 s. The relative mRNA expression was calculated and expressed as $2^{-(\Delta\Delta Ct)}$.

PCR primers were designed using the software PRIMER3 (http://frodo.wi.mit.edu/primer3/) with published sequence data obtained from the NCBI database. Primers were as follows:

hGAPDH: GAAGGTGAAGGTCGGAGT and CATGGGTGGAATCAT ATTGGAA;

hPXR: AGCTGGAACCATGCTGACTT and CACATACACGGCAGA TTTG;

hCYP3a4: CAAGACCCCTTTGTGGAAAA and CGAGGCGACTTTCTT TCATC.

4.5. Statistical analysis

Computation of EC_{50} or IC_{50} values and statistics were performed using Graph Pad Prism 3 software. All values are expressed as the mean ± SD. Comparisons of more than 2 groups were made with the one-way analysis of variance with post-hoc Tukey tests. Differences were considered statistically significant if p was <0.05.

4.6. Molecular modelling

4.6.1. 3D similarity

Molecular overlays of solomonsterols B and **10**, as well as of bazedoxifene-based antagonist (**I**) and **2** were performed with ROCS (OpenEyeScientific Software, Inc.) [45–47]. Prior to ROCS calculation, conformer libraries for compounds **2** and **11**, were generated by OMEGA (OpenEye Scientific Software, Inc.) [55–57]. Solomonsterol B or bazedoxifene-based antagonist (**I**) was used as a query in ROCS and the OMEGA-generated conformer library of **2** or **10** was used as a compound database, respectively. ROCS overlays the chemical structures with the query structure and then compares their shapes (*shape score*) and the chemical types of their atoms (expressed as color, *color score*). Compound conformations were ranked by TanimotoCombo score, which is a combination of shape and color similarities. The highest ranked conformation was used for representation.

4.6.2. Molecular docking

4.6.2.1. Ligand and protein preparation. The three-dimensional models of compounds **1**–**12** were built in ChemBio3D Ultra 13.0. The geometry of the molecules was optimized using MMFF94 [58] force field and partial atomic charges. The energy was minimized until the gradient value was smaller than 0.001 kcal/(mol Å). The optimized structure was further refined with GAMESS interface in ChemBio3D Ultra 13.0 using semiempirical PM3 method, QA optimization algorithm and Gasteiger Hückel charges for all atoms for 100 steps [59]. Molecular docking calculations were performed using GOLD program version 5.2 [49]. Hyperforin and water molecules were deleted from the crystal structure of PXR-hyperforin complex (PDB code: 1M13), and hydrogen atoms were added to the protein using GOLD. The amino acid residues within a radius of 8 Å around the hyperforin were defined as the ligand-binding site.

4.6.2.2. Ligand docking. Compounds **1**–**12** were docked in 25 independent GA runs. The GA parameters were set as suggested by GOLD 5.2. CHEMPLP [50] was used as scoring function. Ten best ranked docking solutions were inspected visually and the best ranked GOLD-calculated conformation was used for analysis and representation. The figures were prepared by PyMOL [51].

Acknowledgments

This work was supported by the European Union FP7 Integrated Project MAREX: Exploring Marine Resources for Bioactive Compounds: From Discovery to Sustainable Production and Industrial Applications (Project No. FP7-KBBE-2009-3-245137) and Slovenian Research Agency (Programme P1-0208). We thank OpenEye Scientific Software, Santa Fe, NM., for free academic licenses for the use of their software.

Appendix A. Supplementary data

Supplementary data related to this article can be found at http://dx.doi.org/10.1016/j.ejmech.2015.09.005.

References

[1] M. Pawlak, P. Lefebvre, B. Staels, General molecular biology and architecture of nuclear receptors, Curr. Top. Med. Chem. 12 (2012) 486–504.
[2] J.L. Staudinger, B. Goodwin, S.A. Jones, D. Hawkins-Brown, K.I. MacKenzie, A. Latour, Y.P. Liu, C.D. Klaassen, K.K. Brown, J. Reinhard, T.N. Willson, B.H. Koller, S.A. Kliewer, The nuclear receptor PXR is a lithocholic acid sensor that protects against liver toxicity, Proc. Natl. Acad. Sci. U. S. A. 98 (2001) 3369–3374.
[3] C.J. Xu, C.Y.T. Li, A.N.T. Kong, Induction of phase I, II and III drug metabolism/transport by xenobiotics, Arch. Pharm. Res. 28 (2005) 249–268.
[4] N. Albermann, F.H. Schmitz-Winnenthal, K. Z'Graggen, C. Volk, M.M. Hoffmann, W.E. Haefeli, J. Weiss, Expression of the drug transporters MDR1/ABCB1, MRP1/ABCC1, MRP2/ABCC2, BCRP/ABCG2, and PXR in peripheral blood mononuclear cells and their relationship with the expression in intestine and liver, Biochem. Pharmacol. 70 (2005) 949–958.
[5] Y.E. Timsit, M. Negishi, CAR and PXR: the xenobiotic-sensing receptors, Steroids 72 (2007) 231–246.
[6] S. Fiorucci, E. Distrutti, G. Bifulco, M.V. D'Auria, A. Zampella, Marine sponge steroids as nuclear receptor ligands, Trends Pharmacol. Sci. 33 (2012) 591–601.
[7] R.E. Watkins, J.M. Maglich, L.B. Moore, G.B. Wisely, S.M. Noble, P.R. Davis-Searles, M.H. Lambert, S.A. Kliewer, M.R. Redinbo, 2.1 angstrom crystal structure of human PXR in complex with the St. John's wort compound hyperforin, Biochemistry 42 (2003) 1430–1438.
[8] S. Mani, W. Dou, M.R. Redinbo, PXR antagonists and implication in drug metabolism, Drug Metab. Rev. 45 (2013) 60–72.
[9] H.W. Wang, H.Y. Huang, H. Li, D.G. Teotico, M. Sinz, S.D. Baker, J. Staudinger, G. Kalpana, M.R. Redinbo, S. Mani, Activated pregnenolone X-receptor is a target for ketoconazole and its analogs, Clin. Cancer Res. 13 (2007) 2488–2495.
[10] A. Biswas, S. Mani, M.R. Redinbo, M.D. Krasowski, H. Li, S. Ekins, Elucidating the 'Jekyll and Hyde' nature of PXR: the case for discovering antagonists or allosteric antagonists, Pharm. Res. 26 (2009) 1807–1815.
[11] J. Cheng, Y.M. Shah, F.J. Gonzalez, Pregnane X receptor as a target for treatment of inflammatory bowel disorders, Trends Pharmacol. Sci. 33 (2012) 323–330.
[12] Y.M. Shah, X. Ma, K. Morimura, I. Kim, F.J. Gonzalez, Pregnane X receptor activation ameliorates DSS-induced inflammatory bowel disease via inhibition of NF-kappa B target gene expression, Am. J. Physiol. Gastrointest. Liver Physiol. 292 (2007) 1114–1122.

[13] A. Mencarelli, M. Migliorati, M. Barbanti, S. Cipriani, G. Palladino, E. Distrutti, B. Renga, S. Fiorucci, Pregnane X receptor mediates the anti-inflammatory activities of rifaximin on detoxification pathways in intestinal epithelial cells, Biochem. Pharmacol. 80 (2010) 1700–1707.
[14] V. Sepe, R. Ummarino, M.V. D'Auria, A. Mencarelli, C. D'Amore, B. Renga, A. Zampella, S. Fiorucci, Total synthesis and pharmacological characterization of solomonsterol A, a potent marine pregnane X receptor agonist endowed with anti-inflammatory activity, J. Med. Chem. 54 (2011) 4590–4599.
[15] X. Ma, Y.M. Shah, G.L. Guo, T. Wang, K.W. Krausz, J.R. Idle, F.J. Gonzalez, Rifaximin is a gut-specific human pregnane X receptor activator, J. Pharmacol. Exp. Ther. 322 (2007) 391–398.
[16] C. Festa, S. De Marino, M.V. D'Auria, G. Bifulco, B. Renga, S. Fiorucci, S. Petek, A. Zampella, Solomonsterols A and B from *Theonella swinhoei*. The first example of C-24 and C-23 sulfated sterols from a marine source endowed with a PXR agonistic activity, J. Med. Chem. 54 (2011) 401–405.
[17] V. Sepe, R. Ummarino, M.V. D'Auria, B. Renga, S. Fiorucci, A. Zampella, The first total synthesis of solomonsterol B, a marine pregnane X receptor agonist, Eur. J. Org. Chem. 2012 (2012) 5187–5194.
[18] S. De Marino, R. Ummarino, M.V. D'Auria, M.G. Chini, G. Bifulco, C. D'Amore, B. Renga, A. Mencarelli, S. Petek, S. Fiorucci, A. Zampella, 4-Methylenesterols from *Theonella swinhoei* sponge are natural pregnane X receptor agonists and farnesoid X receptor antagonists that modulate innate immunity, Steroids 77 (2012) 484–495.
[19] V. Sepe, C. D'Amore, R. Ummarino, B. Renga, M.V. D'Auria, E. Novellino, A. Sinisi, O. Taglialatela-Scafati, Y. Nakao, V. Limongelli, A. Zampella, S. Fiorucci, Insights on pregnane X receptor modulation. Natural and semi-synthetic steroids from *Theonella* marine sponges, Eur. J. Med. Chem. 73 (2014) 126–134.
[20] V. Sepe, F.S. Di Leva, C. D'Amore, C. Festa, S. De Marino, B. Renga, M.V. D'Auria, E. Novellino, V. Limongelli, L. D'Souza, M. Majik, A. Zampella, S. Fiorucci, Marine and semi-synthetic hydroxysteroids as new scaffolds for pregnane X receptor modulation, Mar. Drugs 12 (2014) 3091–3115.
[21] C. Festa, C. D'Amore, B. Renga, G. Lauro, S. De Marino, M.V. D'Auria, G. Bifulco, A. Zampella, S. Fiorucci, Oxygenated polyketides from *Plakinastrella mamillaris* as a new chemotype of PXR agonists, Mar. Drugs 11 (2013) 2314–2327.
[22] L. Xiao, E. Nickbarg, W. Wang, A. Thomas, M. Ziebell, W.W. Prosise, C.A. Lesburg, S.S. Taremi, V.L. Gerlach, H.V. Le, K.C. Cheng, Evaluation of in vitro PXR-based assays and in silico modeling approaches for understanding the binding of a structurally diverse set of drugs to PXR, Biochem. Pharmacol. 81 (2011) 669–679.
[23] J.M. Pascussi, L. Drocourt, J.M. Fabre, P. Maurel, M.J. Vilarem, Dexamethasone induces pregnane X receptor and retinoid X receptor-alpha expression in human hepatocytes: synergistic increase of CYP3A4 induction by pregnane X receptor activators, Mol. Pharmacol. 58 (2000) 361–372.
[24] S.A. Jones, L.B. Moore, J.L. Shenk, G.B. Wisely, G.A. Hamilton, D.D. McKee, N.C.O. Tomkinson, E.L. LeCluyse, M.H. Lambert, T.M. Willson, S.A. Kliewer, J.T. Moore, The pregnane x receptor: a promiscuous xenobiotic receptor that has diverged during evolution, Mol. Endocrinol. 14 (2000) 27–39.
[25] R.E. Watkins, G.B. Wisely, L.B. Moore, J.L. Collins, M.H. Lambert, S.P. Williams, T.M. Willson, S.A. Kliewer, M.R. Redinbo, The human nuclear xenobiotic receptor PXR: structural determinants of directed promiscuity, Science 292 (2001) 2329–2333.
[26] Y.K. Chen, D.T. Nie, Pregnane X receptor and its potential role in drug resistance in cancer treatment, Recent Pat. Anticancer Drug Discov. 4 (2009) 19–27.
[27] Y. Miki, T. Suzuki, K. Kitada, N. Yabuki, R. Shibuya, T. Moriya, T. Ishida, N. Ohuchi, B. Blumberg, H. Sasano, Expression of the steroid and xenobiotic receptor and its possible target gene, organic anion transporting polypeptide-A, in human breast carcinoma, Cancer Res. 66 (2006) 535–542.
[28] D. Gupta, M. Venkatesh, H.W. Wang, S. Kim, M. Sinz, G.L. Goldberg, K. Whitney, C. Longley, S. Mani, Expanding the roles for pregnane X receptor in cancer: proliferation and drug resistance in ovarian cancer, Clin. Cancer Res. 14 (2008) 5332–5340.
[29] H. Masuyama, H. Nakatsukasa, N. Takamoto, Y. Hiramatsu, Down-regulation of pregnane X receptor contributes to cell growth inhibition and apoptosis by anticancer agents in endometrial cancer cells, Mol. Pharmacol. 72 (2007) 1045–1053.
[30] Y. Chen, Y. Tang, M.T. Wang, S. Zeng, D. Nie, Human pregnane x receptor and resistance to chemotherapy in prostate cancer, Cancer Res. 67 (2007) 10361–10367.
[31] C. Raynal, J.M. Pascussi, G. Legueline, C. Breuker, J. Kantar, B. Lallemant, S. Poujol, C. Bonnans, D. Joubert, F. Hollande, S. Lumbroso, J.P. Brouillet, A. Evrard, Pregnane X receptor (PXR) expression in colorectal cancer cells restricts irinotecan chemosensitivity through enhanced SN-38 glucuronidation, Mol. Cancer 9 (2010) 46.
[32] E.J. Mensah-Osman, D.G. Thomas, M.M. Tabb, J.M. Larios, D.R. Hughes, T.J. Giordano, M.L. Lizyness, J.M. Rae, B. Blumberg, P.F. Hollenberg, L.H. Baker, Expression levels and activation of a PXR variant are directly related to drug resistance in osteosarcoma cell lines, Cancer 109 (2007) 957–965.
[33] N. Ouyang, S. Ke, N. Eagleton, Y. Xie, G. Chen, B. Laffins, H. Yao, B. Zhou, Y. Tian, Pregnane X receptor suppresses proliferation and tumourigenicity of colon cancer cells, Brit. J. Cancer 102 (2010) 1753–1761.
[34] T.W. Synold, I. Dussault, B.M. Forman, The orphan nuclear receptor SXR coordinately regulates drug metabolism and efflux, Nat. Med. 7 (2001) 584–590.
[35] L. Krausova, L. Stejskaova, H.W. Wang, R. Vrzal, Z. Dvorak, S. Mani, P. Pavek, Metformin suppresses pregnane X receptor (PXR)-regulated transactivation of CYP3A4 gene, Biochem. Pharmacol. 82 (2011) 1771–1780.
[36] S. Mani, W. Dou, M.R. Redinbo, PXR antagonists and implication in drug metabolism, Drug Metab. Rev. 45 (2013) 60–72.
[37] Ž. Hodnik, L. Peterlin Mašič, T. Tomašić, D. Smodiš, C. D'Amore, S. Fiorucci, D. Kikelj, Bazedoxifene scaffold-based mimetics of solomonsterols A and B as novel pregnane X receptor antagonists, J. Med. Chem. 57 (2014) 4819–4833.
[38] Y. Xue, E. Chao, W.J. Zuercher, T.M. Willson, J.L. Collins, M.R. Redinbo, Crystal structure of the PXR-T1317 complex provides a scaffold to examine the potential for receptor antagonism, Bioorg. Med. Chem. 15 (2007) 2156–2166.
[39] H.W. Wang, H. Li, L.B. Moore, M.D.L. Johnson, J.M. Maglich, B. Goodwin, O.R.R. Ittoop, B. Wisely, K. Creech, D.J. Parks, J.L. Collins, T.M. Willson, G.V. Kalpana, M. Venkatesh, W. Xie, S.Y. Cho, J. Roboz, M. Redinbo, J.T. Moore, S. Mani, The phytoestrogen coumestrol is a naturally occurring antagonist of the human pregnane x receptor, Mol. Endocrinol. 22 (2008) 838–857.
[40] D.M. Tanenbaum, Y. Wang, S.P. Williams, P.B. Sigler, Crystallographic comparison of the estrogen and progesterone receptor's ligand binding domains, Proc. Natl. Acad. Sci. U. S. A. 95 (1998) 5998–6003.
[41] A.K. Shiau, D. Barstad, P.M. Loria, L. Cheng, P.J. Kushner, D.A. Agard, G.L. Greene, The structural basis of estrogen receptor/coactivator recognition and the antagonism of this interaction by tamoxifen, Cell 95 (1998) 923–937.
[42] O. Kuzbari, C.M. Peterson, M.R. Franklin, L.B. Hathaway, E.B. Johnstone, A.O. Hammoud, J.G. Lamb, Comparative analysis of human CYP3A4 and rat CYP3A1 induction and relevant gene expression by bisphenol A and diethylstilbestrol: Implications for toxicity testing paradigms, Reprod. Toxicol. 37 (2013) 24–30.
[43] B. Blumberg, W. Sabbagh, H. Juguilon, J. Bolado, C.M. van Meter, E.S. Ono, R.M. Evans, SXR, a novel steroid and xenobiotic-sensing nuclear receptor, Genes Dev. 12 (1998) 3195–3205.
[44] W. Mnif, J.-M. Pascussi, A. Pillon, A. Escande, A. Bartegi, J.-C. Nicolas, V. Cavailles, M.-J. Duchesne, P. Balaguer, Estrogens and antiestrogens activate hPXR, Toxicol. Lett. 170 (2007) 19–29.
[45] J.A. Grant, M.A. Gallardo, B.T. Pickup, A fast method of molecular shape comparison: a simple application of a Gaussian description of molecular shape, J. Comput. Chem. 17 (1996) 1653–1666.
[46] P.C.D. Hawkins, A.G. Skillman, A. Nicholls, Comparison of shape-matching and docking as virtual screening tools, J. Med. Chem. 50 (2007) 74–82.
[47] *ROCS* 3.2.0.4: OpenEye Scientific Software, Santa Fe, NM. http://www.eyesopen.com.
[48] J.E. McMurry, M.P. Fleming, New method for reductive coupling of carbonyls to olefins. Synthesis of beta-carotene, J. Am. Chem. Soc. 96 (1974) 4708–4709.
[49] *Gold*, v5.2; The Cambridge Crystallographic Data Centre, 12 Union Road, Cambridge, CB2 1EZ, UK, www.ccdc.cam.ac.uk.
[50] O. Korb, T. Stutzle, T.E. Exner, Empirical scoring functions for advanced protein-ligand docking with PLANTS, J. Chem. Inf. Model 49 (2009) 84–96.
[51] PyMOL, Delano Scientific LLC, San Francisco, CA, http://pymol.sourceforge.net.
[52] G.B. Tremblay, T. Kunath, D. Bergeron, L. Lapointe, C. Champigny, J.A. Bader, J. Rossant, V. Giguere, Diethylstilbestrol regulates trophoblast stem cell differentiation as a ligand of orphan nuclear receptor ERR beta, Genes Dev. 15 (2001) 833–838.
[53] S. Di Micco, B. Renga, A. Carino, M.V. D'Auria, A. Zampella, R. Riccio, S. Fiorucci, G. Bifulco, Structural insights into estrogen related Receptor-β modulation: 4-Methylenesterols from *Theonella swinhoei* sponge as the first example of marine natural antagonists, Steroids 80 (2014) 51–63.
[54] G.M. Anstead, K.E. Carlson, J.A. Katzenellenbogen, The estradiol pharmacophore: ligand structure-estrogen receptor binding affinity relationships and a model for the receptor binding site, Steroids 62 (1997) 268–303.
[55] P.C.D. Hawkins, A.G. Skillman, G.L. Warren, B.A. Ellingson, M.T. Stahl, Conformer generation with OMEGA: algorithm and validation using high quality structures from the protein Databank and Cambridge structural database, J. Chem. Inf. Model 50 (2010) 572–584.
[56] P.C.D. Hawkins, A.N. Nicholls, Conformer generation with OMEGA: learning from the dataset and analysis of failures, J. Chem. Inf. Model 52 (2012) 2919–2936.
[57] *OMEGA* 2.5.1.4: OpenEye Scientific Software, Santa Fe, NM. http://www.eyesopen.com.
[58] T.A. Halgren, Merck molecular force field .1. Basis, form, scope, parameterization, and performance of MMFF94, J. Comput. Chem. 17 (1996) 490–519.
[59] GAMESS Interface for ChemBio3D Ultra 13.0 and ChemBioOffice Ultra 13.0; CambridgeSoft: Cambridge, MA.